Linear Polarization Resistance Sensor Using the Structure as a Working Electrode

Douglas W. Brown[1], Richard J. Connolly[2], Duane R. Darr[3] and Bernard Laskowski[4]

[1,2,3,4] *Analatom, Inc., 3210 Scott Blvd., Santa Clara, CA 95054, USA*
douglas.brown@analatom.com
richard.connolly@analatom.com
duane.darr@analatom.com
bernard.laskowski@analatom.com

ABSTRACT

A direct method of measuring corrosion on a structure using a micro-linear polarization resistance (μLPR) sensor is presented. The sensor includes three electrodes, where each electrode is fabricated on a flexible substrate to create a circuit consisting of gold-plated copper. The first two electrodes, or the counter and reference electrodes, are configured in an interdigitated fashion with a separation distance of 8 mil. The flex cable contains a porous membrane between the pair of electrodes and the structure. A third electrode, or the working electrode makes electrical contact to the structure through a 1 mil thick electrically conductive transfer tape placed between the electrode and structure. The reference and counter electrodes are electrically isolated from the working electrode and physically separated from the surface of the structure by 1 mil. The flex cable can be attached to the structure through the use of adhesives or in the case of placement in a butt joint or lap joint configuration, by the joint itself. Corrosion is computed from known physical constants, by measuring the polarization resistance between the electrolytic solution and the structure. A controlled experiment using the ASTM G85 Annex 5 standard verifies the precision and accuracy of sensor measurements by comparing the estimated mass loss with witness coupons.

1. INTRODUCTION

Recent studies have exposed the generally poor state of our nation's critical infrastructure that has resulted from wear and tear under excessive operational loads and environmental conditions. SHM (Structural Health Monitoring) Systems aim at reducing the cost of maintaining high value structures by moving from SBM (Scheduled Based Maintenance) to CBM (Condition Based Maintenance) schemes (Huston, 2010). These systems must be low-cost, simple to install with a user interface designed to be easy to operate. To reduce the cost and complexity of such a system a generic interface node using low-powered wireless communications has been developed. This node can communicate with a myriad of common sensors used in SHM. In this manner a structure such as a bridge, aircraft, or ship can be fitted with sensors in any desired or designated location and format without the need for communications and power lines that are inherently expensive and complex to route. Data from these nodes is transmitted to a central communications Personal Computer (PC) for data analysis. An example of this is provided in Figure 1 showing an embedded AN110 SHM system installed on a C-130H aircraft.

Figure 1. AN110 installed on a C-130H

The μLPR presented in this paper improves on existing LPR

technology by using the structure as part of the sensor system. Further improvements are realized by narrowing the separation distance between electrodes, which minimizes the effects due to solution resistance. This enables the μLPR to operate more effectively outside a controlled aqueous environment, such as an electrochemical cell, in a broad range of applications (eg. civil engineering, aerospace, petrochemical).

The remainder of the paper is organized as follows. Section 2 provides the background into different corrosion sensing technologies, LPR theory, and the new 3-electrode μLPR sensor design. Section 3 describes the experimental procedure used to evaluate the new sensor design through a controlled ASTM G85-A5 test. Section 4 presents the results of experimental testing. Finally, the paper is concluded in Section 5 with a summary of the findings and future work.

2. BACKGROUND

Corrosion sensors can be distinguished by the following categories, *direct* or *indirect* and *intrusive* or *non-intrusive*. Direct corrosion monitoring measures a response signal, such as a current or potential, resulting from corrosion. Examples of common direct corrosion monitoring techniques are: corrosion coupons, electrical resistance (ER), electrochemical impedance spectroscopy (EIS), and linear polarization resistance (LPR) techniques. Whereas, indirect corrosion monitoring techniques measure an outcome of the corrosion process. Two of the most common indirect techniques are ultrasonic testing and radiography. An intrusive measurement requires access to the structure. Corrosion coupons, ER, EIS, and LPR probes are intrusive since they have to access the structure. Non-intrusive techniques include ultrasonic testing and radiography.

Each of these methods have advantages and disadvantages. Corrosion coupons provide the most reliable physical evidence possible. Unfortunately, coupons usually require significant time in terms of labor and provide time averaged data that can not be utilized for real-time or on-line corrosion monitoring (Harris, Mishon, & Hebbron, 2006). ER probes provide a basic measurement of metal loss, but unlike coupons, the value of metal loss can be measured at any time, as frequently as required, while the probe is *in situ* and permanently exposed to the structure. The disadvantage is ER probes require calibration with material properties of the structure to be monitored. The advantage of the LPR technique is that the measurement of corrosion rate is made instantaneously. This is a more powerful tool than either coupons or ER where the fundamental measurement is metal loss and some period of exposure is required to determine corrosion rate. The disadvantage to the LPR technique is that it can only be successfully performed in relatively clean aqueous electrolytic environments (*Introduction to Corrosion Monitoring*, 2012). EIS is a very powerful technique that can provide a corrosion rate and classification of the corrosion mechanism. Disadvantage with EIS is sophisticated instrumentation in a controlled setting is required to obtain an accurate spectrum. In fielded environments, EIS is susceptible to noise. Additionally, interpretation of the data can be difficult (Buchheit, Hinkebein, Maestas, & Montes, 1998). Finally, ultrasonic testing and radiography can be used to detect and measure (depth) corrosion through non-destructive and non-intrusive means (Twomey, 1997). The disadvantage with the ultrasonic testing and radiography equipment is the same with corrosion coupons, both require significant time in terms of labor and can not be utilized for real-time or on-line corrosion monitoring.

2.1. LPR Theory

Corrosion occurs as a result of oxidation and reduction reactions occurring at the interface of a metal and an electrolyte solution. This process occurs by electrochemical half-reactions; (1) anodic (oxidation) reactions involving dissolution of metals in the electrolyte and release of electrons, and (2) cathodic (reduction) reactions involving gain of electrons by the electrolyte species like atmospheric oxygen, O_2, H_2O, or H+ ions in an acid (Harris et al., 2006). The flow of electrons from the anodic reaction sites to the cathodic reaction sites creates a corrosion current. The electrochemically generated corrosion current can be very small (on the order of nanoamperes) and difficult to measure directly. Application of an external potential exponentially increases the anodic and cathodic currents, which allows instantaneous corrosion rates to be extracted from the polarization curve. Extrapolation of these polarization curves to their linear region provides an indirect measure of the corrosion current, which is then used to calculate the rate of corrosion (Burstein, 2005).

The electrochemical technique of LPR is used to study corrosion processes since the corrosion reactions are electrochemical reactions occurring on the metal surface. Modern corrosion studies are based on the concept of mixed potential theory postulated by Wagner and Traud, which states that the net corrosion reaction is the sum of independently occurring oxidation and reduction (Wagner & Traud, 1938). For the case of metallic corrosion in presence of an aqueous medium, the corrosion process can be written as,

$$\mathrm{M} + z\mathrm{H_2O} \underset{b}{\overset{f}{\leftrightarrow}} \mathrm{M}^{z+} + \frac{z}{2}\mathrm{H_2} + z\mathrm{OH}^-, \tag{1}$$

where z is the number of electrons lost per atom of the metal. This reaction is the result of an anodic (oxidation) reaction,

$$\mathrm{M} \underset{b}{\overset{f}{\leftrightarrow}} \mathrm{M}^{z+} + ze^-, \tag{2}$$

and a cathodic (reduction) reaction,

$$z\mathrm{H_2O} + ze^- \underset{b}{\overset{f}{\leftrightarrow}} \frac{z}{2}\mathrm{H_2} + z\mathrm{OH}^- \tag{3}$$

It is assumed that the anodic and cathodic reactions occur at a number of sites on a metal surface and that these sites change in a dynamic statistical distribution with respect to location and time. Thus, during corrosion of a metal surface, metal ions are formed at anodic sites with the loss of electrons and these electrons are then consumed by water molecules to form hydrogen molecules. The interaction between the anodic and cathodic sites as described on the basis of mixed potential theory is represented by well-known relationships using current (reaction rate) and potential (driving force). For the above pair of electrochemical reactions (2) and (3), the relationship between the applied current I_a and applied potential, E_a, follows the Butler-Volmer equation,

$$I_a = I_{corr}\left[e^{2.303(E_a-E_{corr})/\beta_a} - e^{-2.303(E_a-E_{corr})/\beta_c}\right], \quad (4)$$

where β_a and β_c are the anodic and cathodic Tafel parameters given by the slopes of the polarization curves $\partial E_a/\partial \log_{10} I_a$ in the anodic and cathodic Tafel regimes, respectively and E_{corr} is the corrosion, or open circuit potential (Bockris, Reddy, & Gambola-Aldeco, 2000). The corrosion current, I_{corr}, cannot be measured directly. However, *a priori* knowledge of β_a and β_c along with a small signal analysis technique, known as polarization resistance, can be used to indirectly compute I_{corr}. The polarization resistance technique, also referred to as linear polarization, is an experimental electrochemical technique that estimates the small signal changes in I_a when E_a is perturbed by $E_{corr} \pm 10\text{mV}$ (G102, 1994). The slope of the resulting curve over this range is the polarization resistance,

$$R_p \triangleq \left.\frac{\partial E_a}{\partial I_a}\right|_{|E_a-E_{corr}|\leq 10\text{mV}}. \quad (5)$$

ASTM standard G59 outlines procedures for measuring polarization resistance. Potentiodynamic, potential step, and current-step methods can be used to compute R_p (G59, 1994). The potentiodynamic sweep method is the most common method for measuring R_p. A potentiodynamic sweep is conducted by applying E_a between $E_{corr} \pm 10\text{mV}$ at a slow scan rate, typically $0.125\,\text{mV/s}$. A linear fit of the resulting E_a vs. I_a curve is used to compute R_p. Note, the applied current, I_a, is the total applied current and is not multiplied by the electrode area so R_p as defined in (5) has units of Ω. Provided that $|E_a - E_{corr}|/\beta_a \ll 1$ and $|E_a - E_{corr}|/\beta_c \ll 1$, the first order Taylor series expansion $e^x \cong 1 + x$ can be applied to (4) and (5) to arrive at the Stern-Geary equation,

$$I_{corr} = \frac{B^\star}{R_p}, \quad (6)$$

where,

$$B^\star = \frac{\beta_a \beta_c}{2.303\,(\beta_a + \beta_c)} \quad (7)$$

Knowledge of R_p, β_a, and β_c enables direct determination of I_{corr} at any instant in time. The corrosion rate, R_{loss}, can be found by applying Faraday's law,

$$R_{loss}(t) = \frac{B_{corr}}{R_p(t)}, \quad (8)$$

where,

$$B_{loss} = \frac{B^\star}{FA_{sen}}\left(\frac{AW}{z}\right), \quad (9)$$

such that F is Faraday's constant, z is the number of electrons lost per atom of the metal during an oxidation reaction, A_{sen} is the effective area of the sensor, and AW is atomic weight. The total mass loss, M_{loss}, due to corrosion can be found by integrating (8),

$$M_{loss}(t) = \int_{t_0}^{t} R_{loss}(\tau)\, d\tau. \quad (10)$$

Finally, since R_p is not measured continuously (10) needs to be discretized for the sample period T_s,

$$\left.M_{loss}(t)\right|_{t=NT_s} = T_s \sum_{k=1}^{N} R_{loss}(kT_s) \quad (11)$$

2.2. Sensor Design

Each electrode is fabricated on a flexible substrate to create a circuit consisting of a noble metal, typically gold-plated copper. The first two electrodes, counter and reference electrodes, are fabricated with a thickness of 2 mil configured in a interdigitated geometric layout with a separation distance of 8 mil. The flex cable contains an insulated / porous scrim material between the pair of electrodes and the structure. A third electrode, or working electrode, is placed in close proximity to the counter and reference electrodes and makes electrical contact to the structure by placing a 1 mil thick electrically conductive transfer tape between the electrode and structure. The flex cable, shown in Figure 2, can be attached to the structure through the use of adhesives or in the case of placement in a butt joint or lap joint configuration, the holding force is provided by the joint itself. Corrosion is computed by measuring the polarization resistance between the electrolytic solution and the structure using the three electrodes and applying (11).

3. EXPERIMENTAL PROCEDURES

3.1. Tafel Measurements

ASTM standard G59 outlines the procedure for measuring the Tafel slopes, β_a and β_c. First, E_{corr} is measured from the open circuit potential. Next, E_a is initialized to E_corr-250mV. Then, a potentiodynamic sweep is conducted by increasing E_a from $E_{corr} - 250\text{mV}$ to $E_{corr} + 250\text{mV}$ at a slow scan rate, typically $0.125\,\text{mV/s}$. Finally, a Tafel curve is plotted for E_a vs. $\log_{10} I_a$. Values for β_a and β_c are estimated

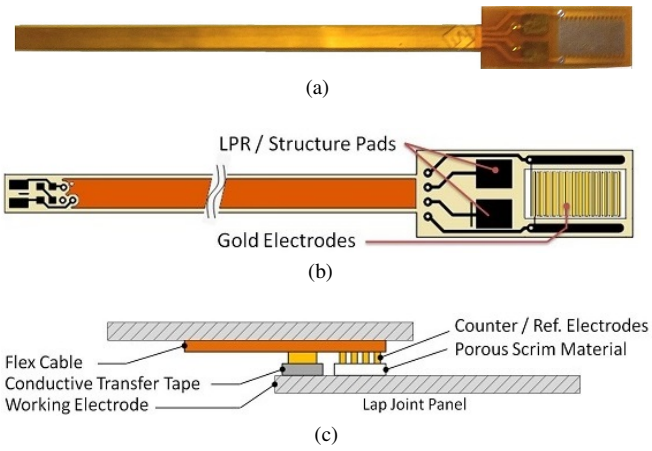

Figure 2. The μLPR sensor (a) as fabricated on a flexible circuit, (b) illustration identifying each electrode, and (c) using the structure as the third electrode.

from the slopes of the linear extrapolated anodic and cathodic currents.

3.2. Sample Preparation

New samples were cut to length and uniquely stamped with stencils close to the edge of both faces of the sample. The samples were then cleaned using an alkaline cleaner, TURCO 4215 NC-LT – 50 g/L for 35 min at 65°C. Afterward, the samples were rinsed with Type IV reagent grade deionized water and immersed in a solution of 70% (v/v) nitric acid for 5 min. The samples were then rinsed again in the deionized water and air dried. The weights were recorded to the nearest fifth significant figure and the samples were stored in a desiccator. After massing, the samples were assembled in a lap-joint configuration and coated with 2 mil of epoxy-based primer and 2 mil of polyurethane.

3.3. Accelerated Testing

Corrosion tests were performed in a cyclic corrosion chamber running the ASTM G85-A5 test. This test consisted of two one-hour steps. The first step involved exposing the samples to a salt fog for a period of one-hour at 25°C. The electrolyte solution composing the fog was 0.05% sodium chloride and 0.35% ammonium sulfate in deionized water. This step was followed by a dry-off step, where the fog was purged from the chamber while the internal environment was heated to 35°C. Electrical connections for the flex sensors were made to an AN110 positioned outside the sealed chamber by passing extension cables through the bulkhead in the chamber. Temperature, relative humidity, and μLPR data was acquired at 1 min intervals.

3.4. Sample Cleaning

3.4.1. Lap-Joint Panels

Lap joints were removed from the environmental chamber and disassembled. Following disassembly, the polyurethane and epoxy coatings on the aluminum panels were removed by placing them in a solution of methyl ethyl ketone. After immersion for 30 min the panels were removed and rinsed with deionized water. These panels were again alkaline cleaned with a 35 min immersion into a constantly stirred solution of 50 g/L Turco 4215 NC-LT at 65°C. This was followed by a deionized water rinse and immersion into a 90°C solution of 4.25% phosphoric acid containing 20 g/L chromium trioxide for 10 min. Following phosphoric acid treatment the panels were rinsed with deionized water and placed into a 70% nitric acid solution for 5 min at 20°C. Plates were then rinsed with deionized water, dipped in ethanol, and dried with a heat gun. This cleaning process was repeated until mass values for the panels stabilized. These values were then compared with mass loss values calculated from the μLPR data.

3.4.2. Control Coupons

Control samples, free of any corrosion, were weighed before and after being subjected to the same cleaning process as the corroded samples to determine the extent of metal loss resulting from the cleaning procedure. Corroded samples were lightly brushed with nylon bristles. The corroded samples were then placed in a solution of TURCO 4215 NC-LT – 50 g/L for 1 hour at 65°C. Afterward, in accordance with ASTM G1, the standard practice for preparing, cleaning, and evaluating corrosion test specimens, the samples were placed in a 90°C solution of 4.25% phosphoric acid containing 20 g/L chromium trioxide for 10 min. Next, the samples were placed in 70% (v/v) nitric acid for 5 min at 20°C. Following this step the samples were rinsed with deionized water. Finally, the samples were dipped in ethanol, dried, and stored in a desiccator cabinet.

4. RESULTS

This experiment ran over a period of 230 hours, where the environment inside the chamber was varied in temperature and humidity to promote corrosion. Once the experiment began, the Tafel constants were acquired while the panels were undergoing a wetting cycle. The Tafel constants were acquired and plotted as applied voltage vs. the logarithm of the applied current magnitude, shown in Figure 3. From this plot the Tafel constants were computed as, $\beta_a \approx 0.40\,\mathrm{V/dec}$ and $\beta_c \approx 0.15\,\mathrm{V/dec}$. The corrosion constant, B_{loss}, was computed using (9) with the material properties for AA2024-T3 and sensor properties defined in the nomenclature. Panels 1-4 were removed 33, 130, 170, and 230 hours into the experiment, respectively. Plots of the measured temperature and humidity vs. time are provided in Figure 4. The corrosion rate,

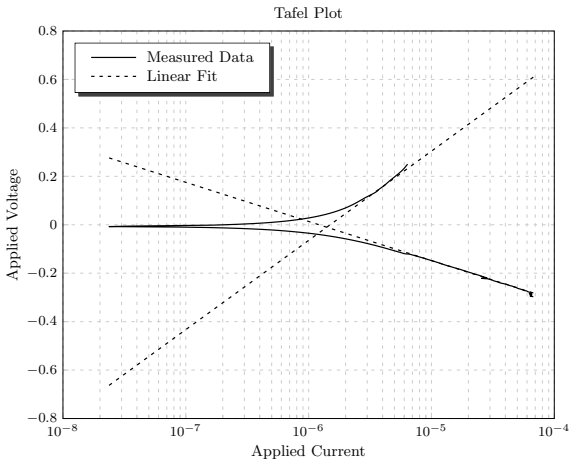

Figure 3. Tafel plot of the μLPR sensors.

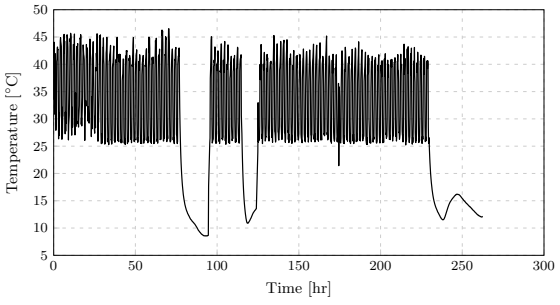

(a)

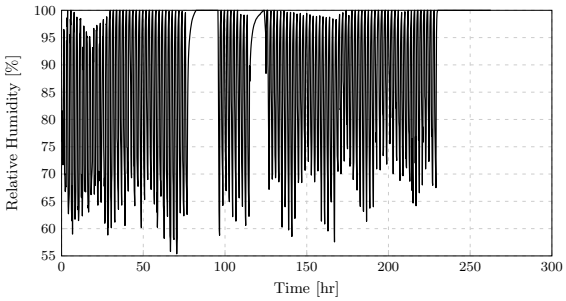

(b)

Figure 4. Plots of (a) temperature and (b) relative humidity vs. time.

shown in Figure 5, was computed from R_p measurements using (8).

The total corrosion, shown in Figure 6, was computed for each panel by applying (10) to integrate the corrosion rate with respect to time. The error bars correspond to the standard deviation observed at the time when the mass loss was computed. Finally, the measured and computed corrosion from the μLPR measurements were compared in a scatter plot, shown in Figure 7. The error bars in the y-direction correspond to observation error. These results indicate the measured corrosion correlated with the computed corrosion to within 95% confidence (two standard deviations of the observation error).

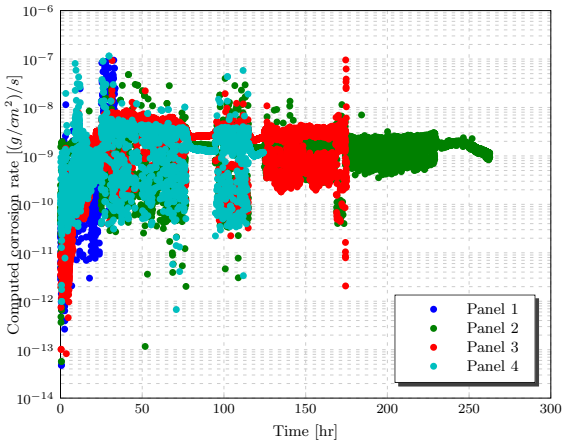

Figure 5. Computed corrosion rate vs. time.

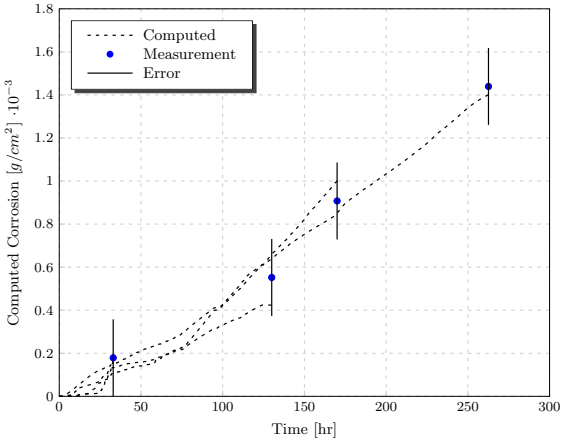

Figure 6. Computed corrosion vs. time.

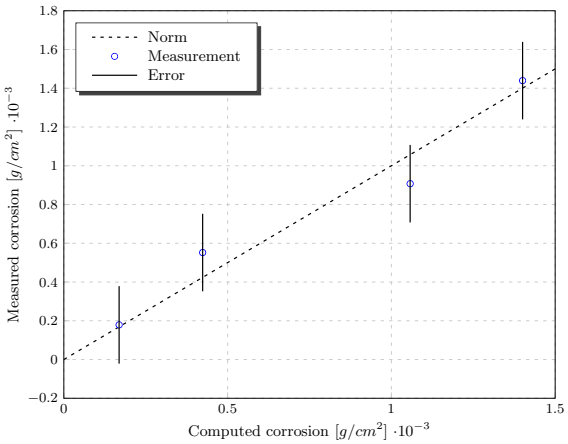

Figure 7. Measured vs. computed corrosion.

5. CONCLUSION

A new μLPR sensor design was presented for direct corrosion monitoring in Structural Health Management (SHM) applications. The new design improves on existing technologies by (1) using the structure as part of the sensor measurement, (2) improving sensor lifetime by making the electrodes from a non-corrosive material, and (3) improving on sensor performance by reducing the separation distance between the working, reference, and counter electrodes. Corrosion tests were performed in a cyclic corrosion chamber running ASTM G85-A5 salt-fog test. The results indicate the μLPR sensor data correlated with the measured mass loss to within 95% confidence (two standard deviations of the observation error). This demonstrates the μLPR sensor can accurately measure the change in the corrosion rate as a function of time for a given electrolyte condition. Future work includes:

- Demonstrate μLPR sensor accurately measures the corrosion rate as a function of solution conductivity. This is important as the environment (in terms of bare metal surfaces) will experience wet-dry cycles.
- Establish the μLPR sensor can accurately measure corrosion in atmospheric conditions where corrosion rates are lower than in an "accelerated corrosion chamber" (i.e. what is the lowest rate of corrosion that the sensors can measure when a monolayer of electrolyte is present).
- Investigate the surface morphology of the coupons using a scanning electron microscope (SEM) and correlate their measured corrosion rate as a function of their corrosion behavior (e.g. pitting vs. uniform corrosion) as determined by the μLPR sensor data over time.

ACKNOWLEDGMENT

All funding and development of the sensors and systems in the project has been part of the US government's SBIR programs. In particular: 1) Funding for the preparation of the initial system design and development was provided by the US Air Force under SBIR Phase II contract # F33615-01-C-5612 monitored by Dr. James Mazza, 2) Funding for the development and experimental set-up was provided by the US Navy under SBIR Phase II contract # N68335-06-C-0317 monitored by Dr. Paul Kulowitch, and 3) further improvements, scheduled field installations, and technology transition by the US Air Force under SBIR Phase II contract # FA8501-11-C-0012 and BAA/RIF contract # FA8650-12-C-0001 monitored by Mr. Feraidoon Zahiri.

NOMENCLATURE

β_a	$^{V}/_{dec}$	0.40	anodic Tafel constant
β_c	$^{V}/_{dec}$	0.15	cathodic Tafel constant
τ	s	-	time variable
$d\tau$	s	-	time step
k	-	-	sample index
t	s	-	time
t_0	s	-	initial time
z	-	3	electron loss
A_{sen}	cm^2	4.233×10^{-2}	sensor area
AW	$^{g}/_{mol}$	2.899×10^{1}	atomic weight
$B^{\star}$	$^{V}/_{dec}$	4.95×10^{-2}	constant
B_{loss}	$^{\Omega \cdot g}/_{cm^2/s}$	1.170×10^{-4}	constant
E_a	V	-	applied potential
E_{corr}	V	-	corrosion potential
I_a	$^{A}/_{cm^2}$	-	applied current
I_{corr}	$^{A}/_{cm^2}$	-	corrosion current
F	$^{C}/_{mol}$	9.649×10^{4}	Faraday's constant
M_{loss}	$^{g}/_{cm^2}$	-	mass loss
N	-	-	total samples
R_{loss}	$^{g}/_{cm^2/s}$	-	corrosion rate
R_p	Ω	-	polarization resistance
T_s	s	60	sample period

REFERENCES

Bockris, J. O., Reddy, A. K. N., & Gambola-Aldeco, M. (2000). *Modern electrochemistry 2a. fundamentals of electrodics* (2nd ed.). New York: Kluwer Academic/Plenum Publishers.

Buchheit, R. G., Hinkebein, T., Maestas, L., & Montes, L. (1998, March 22-27). Corrosion monitoring of concrete-lined brine service pipelines using ac and dc electrochemical methods. In *Corrosion 98.* San Diego, Ca.

Burstein, G. T. (2005, December). A century of tafel's equation: 1905-2005. *Corrosion Science*, *47*(12), 2858-2870.

G102, A. S. (1994). Standard practice for calculation of corrosion rates and related information from electrochemical measurements. *Annual Book of ASTM Standards*, *03.02*.

G59, A. S. (1994). Standard practice for conducting potentiodynamic polarization resistance measurements. *Annual Book of ASTM Standards*, *03.02*.

Harris, S. J., Mishon, M., & Hebbron, M. (2006, October). Corrosion sensors to reduce aircraft maintenance. In *Rto avt-144 workshop on enhanced aircraft platform availability through advanced maintenance concepts and technologies.* Vilnius, Lithuania.

Huston, D. (2010). *Structural sensing, health monitoring, and performance evaluation* (B. Jones & W. B. S. J. Jnr., Eds.). Taylor and Francis.

Introduction to corrosion monitoring. (2012, August 20). Online. Available from `http://www.alspi.com/introduction.htm`

Twomey, M. (1997). Inspection techniques for detecting corrosion under insulation. *Material Evaluation*, *55*(2),

129-133.
Wagner, C., & Traud, W. (1938).
Elektrochem, *44*, 391.

BIOGRAPHIES

Douglas W. Brown is the Senior Systems Engineer for Analatom, Inc. He received the bachelor of science degree in electrical engineering from the Rochester Institute of Technology and his master of science and doctor of philosophy degrees in electrical engineering from the Georgia Institute of Technology. Dr. Brown has eight years of experience developing and maturing Prognostics & Health Management (PHM) and fault-tolerant control systems in avionics application. He is a recipient of the National Defense Science and Engineering Graduate (NDSEG) Fellowship and has received several best-paper awards in his work in PHM and fault-tolerant control.

Richard J. Connolly is the Senior Research Engineer for Analatom, Inc. He completed his bachelor of science and doctor of philosophy degree in chemical and biomedical engineering at the University of South Florida. Dr. Connolly is a fellow of the National Science Foundation and is regarded as an expert in interfacing of engineering devices with skin. He has extensive experience in bioelectrics, electrochemistry, and analysis of biological data. Much of this experience was gained while performing bioelectric data collection on human and animal models. During his tenure at Analatom he has overseen testing and validation of the μLPR technology for aerospace and civil engineering applications.

Duane R. Darr is the Senior Embedded System Engineer at Analatom with over 30 years of experience in the software and firmware engineering fields. He completed his undergraduate work in physics, and graduate work in electrical engineering and computer science at Santa Clara University. Mr. Darr's previous work at Epson Imaging Technology Center, San Jose, California, as Senior Software Engineer, Data Technology Corporation, San Jose, California as Senior Firmware Engineer, and Qume Inc., San Jose, California, as Member of Engineering Staff/Senior Firmware Engineer, focused on generation and refinement of software and firmware solutions for imaging core technologies as well as digital servo controller research, development, and commercialization.

Bernard Laskowski is the President and Senior Research Scientist at Analatom since 1981. He received the licentiaat and doctor of philosophy degrees in physics from the University of Brussels in 1969 and 1974, respectively. Dr. Laskowski has published over 30 papers in international refereed journals in the fields of micro-physics and microchemistry. As president of Analatom, Dr. Laskowski has managed 93 university, government, and private industry contracts, receiving a U.S. Small Business Administration Administrator's Award for Excellence.